

Cite this: *RSC Adv.*, 2019, 9, 12441

# Importance of protein flexibility in ranking ERK2 Type I<sup>1/2</sup> inhibitor affinities: a computational study†

Yuzhen Niu, <sup>\*,a</sup> Xiaojun Yao<sup>b</sup> and Hongfang Ji<sup>\*,a</sup>

Extracellular-regulated kinase (ERK2) has been regarded as an essential target for various cancers, especially melanoma. Recently, pyrrolidine piperidine derivatives were reported as Type I<sup>1/2</sup> inhibitors of ERK2, which occupy both the ATP binding pocket and the allosteric pocket. Due to the dynamic behavior of ERK2 upon the binding of Type I<sup>1/2</sup> inhibitors, it is difficult to predict the binding structures and relative binding potencies of these inhibitors with ERK2 accurately. In this work, the binding mechanism of pyrrolidine piperidines was discussed by using different simulation techniques, including molecular docking, ensemble docking based on multiple receptor conformation, molecular dynamics simulations and free energy calculations. Our computational results show that the traditional docking method cannot predict the relative binding ability of the studied inhibitors with high accuracy, but incorporating ERK2 protein flexibility into docking is an effective method to improve the prediction accuracy. It is worth noting that the binding free energies predicted by MM/GBSA or MM/PBSA based on the MD simulations for the docked poses have the highest correlation with the experimental data, which highlights the importance of protein flexibility for accurately predicting the binding ability of Type I<sup>1/2</sup> inhibitors of ERK2. In addition, the comprehensive analysis of several representative inhibitors indicates that hydrogen bonds and hydrophobic interactions are of significance for improving the binding affinities of the inhibitors. We hope this work will provide valuable information for further design of novel and efficient Type I<sup>1/2</sup> ERK2 inhibitors.

Received 5th March 2019  
Accepted 9th April 2019

DOI: 10.1039/c9ra01657k

rsc.li/rsc-advances

## 1. Introduction

The Ras/MAPK (RAF/MEK/ERK) signaling transduction is a key pathway of cellular proliferation, differentiation and survival downstream of RAS activation.<sup>1–3</sup> Not surprisingly, this pathway is frequently deregulated in human cancers, such as melanoma.<sup>4,5</sup> The extracellular-regulated kinases (ERK1 and ERK2) are central in the pathway downstream of Ras, Raf, and MEK kinases, while ERK1 and ERK2 show 89% sequence identity within the kinase domains. Activation/phosphorylation of ERK promotes tumor growth, cell cycle progression and survival through transcriptional activation, for example, ERK1/2 was found constitutively activated in 60% of melanoma cells.<sup>6</sup> Therefore, the ERK1/2 kinase is the central node of the RAS/MAPK pathway. The greatest advantage of targeting ERK1/2 is that no mutations have been found in ERK1/2.<sup>7,8</sup>

Despite ERK1/2 inhibitors playing an important role in the MAPK pathway, few ERK1/2 inhibitors have been reported in the

literature, and no known ERK1/2 inhibitor has entered advanced clinical trials.<sup>9–11</sup> So, development of potential ERK1/2 inhibitors is extremely urgent. The majority of reported ERK1/2 inhibitors are ATP competitive inhibitors, which belong to Type I kinase inhibitors, such as VTX-11e,<sup>10</sup> FR180204 (ref. 12) and GDC-0994.<sup>13</sup> Apirat *et al.* reported that inhibitor SCH772984 simultaneously binds to the ATP binding pocket and the allosteric pocket. The allosteric pocket is adjacent to the ATP binding pocket, which located between P-loop and  $\alpha$ C helix. As a Type I<sup>1/2</sup> kinase inhibitor, SCH772984 is a promising inhibitor targeting ERK1/2 with high bioactivity, and we have previously studied the interaction mechanisms of SCH772984 with ERK2.<sup>14</sup> Afterwards, Deng and coworkers discovered compound **1** as an effective selective ERK2 inhibitor through the automated ligand identification system (ALIS),<sup>15</sup> and meanwhile they obtained the crystal structure of human ERK2 bound compound **1** (PDB ID: 4QYY<sup>16</sup>). As shown in Fig. 1, the binding mode of compound **1** to ERK2 is similar with that of SCH772984 to ERK2. In detail, ERK2 adapts a “DFG in” mode, and compound **1** forms hydrogen-bonding interaction with the residues Lys52, Gln103, Asp104 and Met106. Chlorophenyl forms hydrophobic interaction with the hinge region and catalytic loop region of ERK2. Besides, the acetyl phenyl interacts “face to face” with the Tyr62 side chain through an aromatic  $\pi$ – $\pi$  interaction, which may be critical to improve the potencies of ERK2 Type I<sup>1/2</sup> inhibitors.

<sup>a</sup>Shandong Provincial Research Center for Bioinformatic Engineering and Technique, College of Life Sciences, Shandong University of Technology, Zibo 255049, China. E-mail: niuyzh12@lzu.edu.cn; jhf@sdu.edu.cn

<sup>b</sup>State Key Laboratory of Applied Organic Chemistry, Department of Chemistry, Lanzhou University, Lanzhou 730000, China

† Electronic supplementary information (ESI) available. See DOI: 10.1039/c9ra01657k



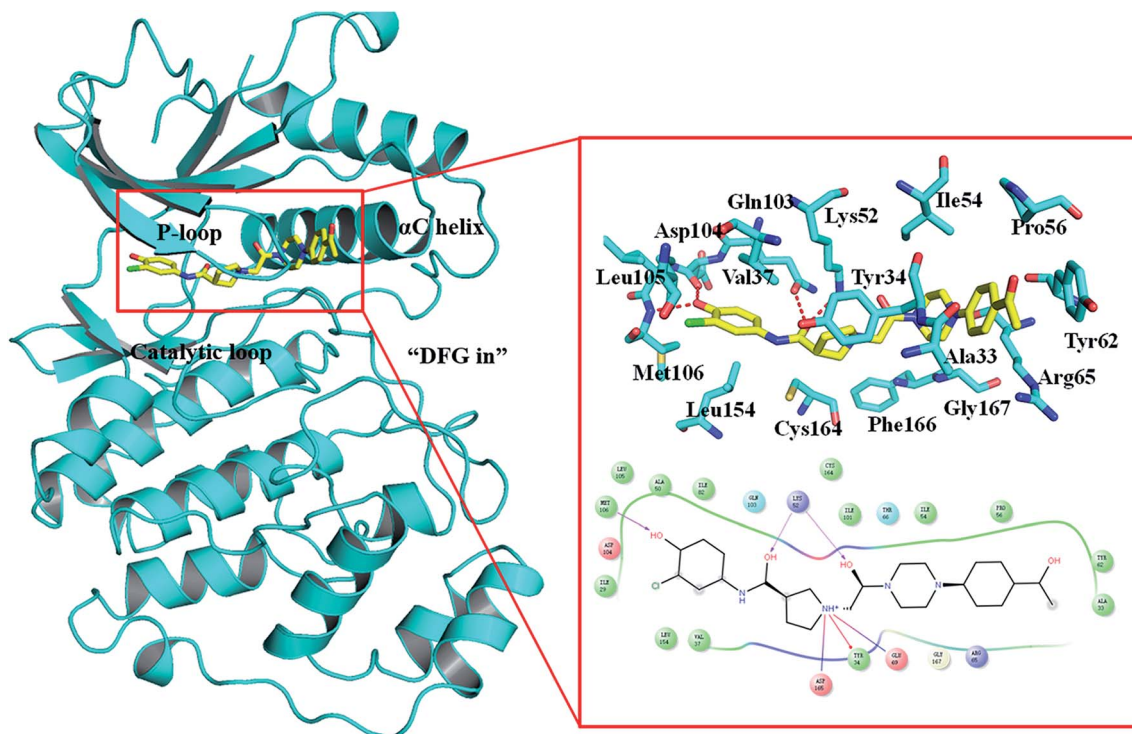


Fig. 1 Binding mode of ERK2 with compound 1. The key residues in the binding pocket of ERK2 and the interactions between compound 1 and ERK2 are highlighted.

Based on the structures of the compounds already reported, investigating the interaction mechanisms of these compounds with ERK2 is of great significance for discovering efficient and potential ERK2 inhibitors. Therefore, in this study, a combined computational modeling strategy, based on molecular docking, molecular dynamics (MD) simulations, free energy calculations and free energy decomposition analysis, was employed to understand the interaction between ERK2 and Type I<sup>1/2</sup> inhibitors and identify several key structures that are important to the efficiency of inhibitors.

The use of rigid protein structures may hinder the correct prediction of ligand binding posture and relative binding capacity due to the dynamic behavior of kinase in binding of Type I<sup>1/2</sup> inhibitors.<sup>17–19</sup> Herein, various molecular modeling techniques were used to handle the flexibility of ERK2, including ensemble docking and MD simulations and induced-fit docking (IFD). IFD simulates the induced fit by refining the side chain conformation of important residues located in active site. Ensemble docking is based on the use of multiple receptor conformation (MRC) in molecular docking to combine protein flexibility.<sup>20,21</sup> In this study, MD simulations and structural generate an ensemble of MRC for ERK2, and then was utilized for ERK2 docking with Type I<sup>1/2</sup> inhibitors. The complex structure of ERK2 with Type I<sup>1/2</sup> inhibitors after docking were carried out MD simulations to get the stable conformations. Then both Molecular Mechanics/Poisson–Boltzmann Surface Area (MM/PBSA) and Molecular Mechanics/Generalized Born Surface Area (MM/GBSA) technologies were employed to predict the binding potencies of these 27 inhibitors with ERK2. We expect that the detailed analysis of the structural and energetic

binding mode of ERK2 and Type I<sup>1/2</sup> inhibitors will provide valuable information for designing novel, effective and selective inhibitors with controllable activity.

## 2. Materials and methods

### 2.1 Preparing systems

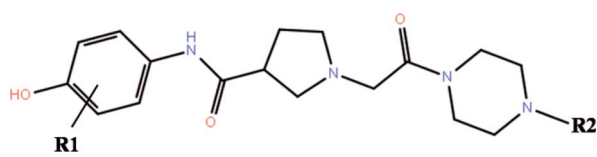
The co-crystallized structures of two known inhibitors bound with ERK2 were retrieved from the RCSB Protein Data Bank (PDB ID codes: 4QTA<sup>22</sup> and 4QYY<sup>16</sup>). The missing residues were added using the Prime module in Schrodinger 2009.<sup>23</sup> After that the two structures were prepared by the Protein Preparation Wizard in Schrodinger 2009, including adding assigning protonation states, side chains of residues and hydrogen atoms, and relaxing the amino residue side chains of the proteins.

The 3D structures of all the 27 inhibitors<sup>16,24</sup> were sketched by Maestro and preprocessed by LigPrep, which generated the low energy 3D conformers for each compound with the OPLS-2005 force field. The ionized state was assigned by using Epik at a target pH value of 7.0 ± 2.0. Default settings were used for the other parameters. The 2D structures of all the 27 compounds and their biological activities against ERK2 are summarized in Table 1.

### 2.2 Generation of multiple representative ERK2 protein conformations

Based on the two resolved crystal structures (PDB codes: 4QTA and 4QYY), the representative ERK2 conformations for ensemble docking were generated by molecular dynamics (MD) simulations. The partial charges of the two inhibitors in

Table 1 Structures, biological activities and predicted scores of the studied ERK2 inhibitors



The image shows the chemical structure of the ERK2 inhibitor core. It consists of a 3-hydroxyphenyl group (R1) attached to an amide group, which is further attached to a pyrrolidine ring. This pyrrolidine ring is connected via a methylene group to another amide group, which is attached to a piperidine ring (R2).

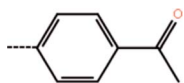
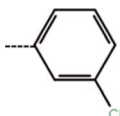
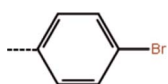
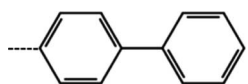
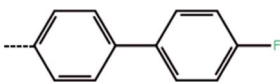
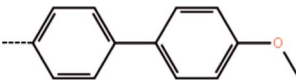
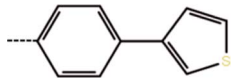
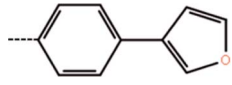
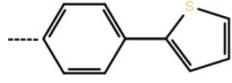
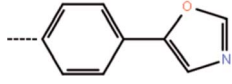
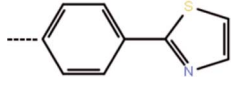
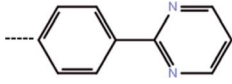
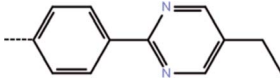
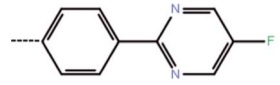
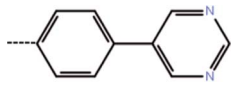
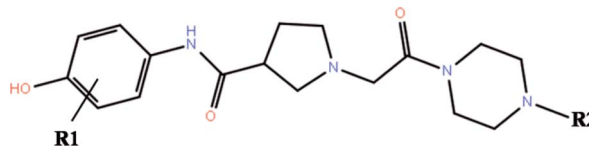
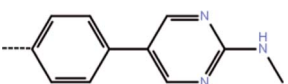
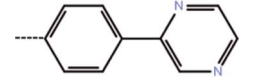
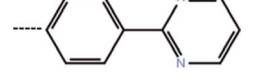
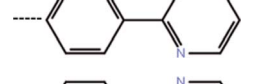
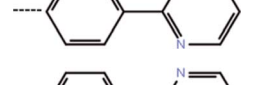
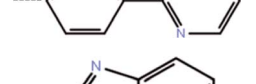
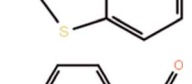

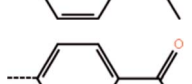
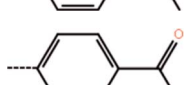
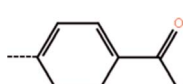

No.	R1	R2	IC <sub>50</sub> <sup>a</sup> (μM)	pIC <sub>50</sub>	RRD	IFD	QPLD
1	3-Cl		2.6	5.58	-13.84	-14.20	-14.11
1a	3-Cl		2.1	5.68	-13.50	-14.09	-13.28
1b	3-Cl		8.2	5.09	-12.97	-12.50	-13.51
2	3-Cl		4.4	5.36	-11.71	-13.37	-17.01
2a	3-Cl		100	4.00	-8.77	-9.59	-14.78
2b	3-Cl		50	4.30	-11.83	-11.98	-11.83
3	3-Cl		20	4.70	-11.30	-13.74	-16.87
3a	3-Cl		5.5	5.26	-11.51	-10.52	-14.75
3b	3-Cl		20	4.70	-11.53	-13.80	-17.27
3c	3-Cl		12	4.92	-10.74	-11.34	-14.66
3d	3-Cl		9.34	5.03	-12.88	-9.33	-14.52
4	3-Cl		0.41	6.39	-13.72	-12.04	-14.58
4a	3-Cl		0.10	7.00	-13.41	-14.08	-16.45
4b	3-Cl		1.76	5.75	-8.28	-9.20	-16.22
5	3-Cl		1.8	5.74	-12.34	-10.10	-14.84

Table 1 (Contd.)



The core molecule is a 2-(4-hydroxyphenyl)propanamide derivative. The amide nitrogen is connected to a proline ring, which is further connected via a methylene group to a piperazine ring. The piperazine ring has an R2 substituent on one of its nitrogens. The phenyl ring of the propanamide part has an R1 substituent at the 3-position and a hydroxyl group at the 4-position.

No.	R1	R2	IC <sub>50</sub> <sup>a</sup> (μM)	pIC <sub>50</sub>	RRD	IFD	QPLD
5a	3-Cl		2.67	5.57	-7.68	-11.97	-16.51
6	3-Cl		0.13	6.89	-12.90	-14.39	-14.65
7	3-CF <sub>3</sub>		0.10	7.00	-14.15	-14.36	-14.95
7a	3-Cyclopropyl		1.76	5.75	-14.44	-14.59	-15.88
7b	3-Isopropyl		1.80	5.74	-13.95	-14.28	-15.76
7c	3-(4-Fluoro phenyl)		2.67	5.57	-7.44	-12.78	-17.33
8	3-Cl		1.6	5.80	-12.18	-12.63	-13.03
9	H		18.6	4.73	-13.17	-10.74	-13.14
9a	2-Cl		50	4.30	-13.32	-12.68	-13.66
9b	3-Br		3.6	5.44	-13.89	-14.96	-14.03
9c	3-F		11.8	4.93	-13.74	-12.91	-14.25
9d	3-Methyl		2.5	5.60	-13.70	-13.53	-14.00

<sup>a</sup> Refer to the ref. 16 and 24.

4QTA and 4QYY were fitted using the RESP methodology based on the electrostatic potentials computed at the HF/6-31G(d) level of theory.<sup>25-27</sup> The AMBER99SB<sup>28</sup> and GAFF force fields were used for the proteins and inhibitors, respectively.<sup>29</sup> Then, Na<sup>+</sup> ions were added to neutralize the net charge of the two complexes, and last the two systems were solvated into a 10 Å cubic TIP3P water<sup>30</sup> box.

All of the MD simulations were performed with the NAMD 2.9 simulation package.<sup>31</sup> The specific parameter settings refer to our previous work.<sup>32</sup> Particle Mesh Ewald (PME) algorithm<sup>33</sup> was employed to treat long-range electrostatic interactions, while the cutoff for the short-range non-bonded interactions were set to 10 Å. All bonds involving hydrogen atoms were restrained using the SHAKE<sup>34</sup>

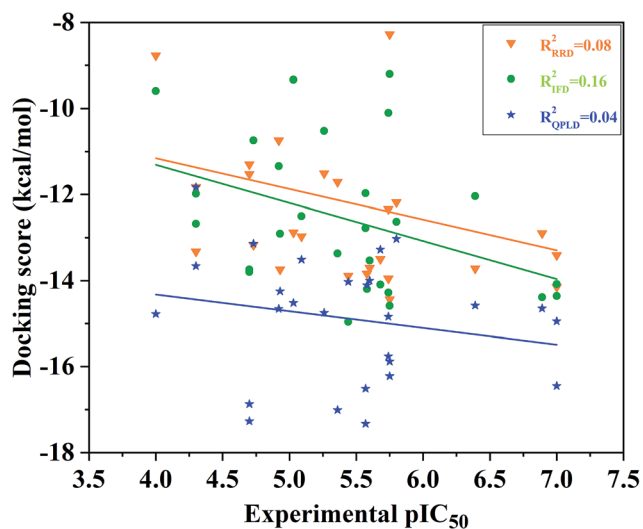


Fig. 2 Correlation between the docking scores predicted by RRD, IFD or QPLD and the experimental data.

algorithm, and the time step was set to 2 fs. During the sampling process, the coordinates of each complex were saved every 1 ps.

For each complex structure, 200 conformations were evenly extracted from the final stable 10 ns MD trajectories, and then clustered into 10 categories using the *k*-means clustering method based on the RMSDs within 5 Å in the ligand binding pocket in the extracted MD conformations. At last, 10 representative structures chosen from 10 clusters were generated.

### 2.3 Docking protocols

According to the two crystal structures 4QTA and 4QYY, the studied 27 inhibitors were docked into the binding pocket of ERK2 using Glide in Schrodinger 9.0. For each system, the binding site was defined based on the known ligand (SCH772984 in 4QTA and compound 1 in 4QYY), and the receptor grid box for docking was set to 25 Å × 25 Å × 25 Å using the Receptor Grid Generation protocol of Schrodinger 9.0. Default settings were used for the other parameters.

**2.3.1 Rigid receptor docking.** During this docking process, the protein was fixed while the inhibitors were flexible. So, the 27 inhibitors were firstly generated some reasonable conformations and then docked into the binding pocket of ERK2 in Glide, and the extra precision (XP) scoring mode was chosen.

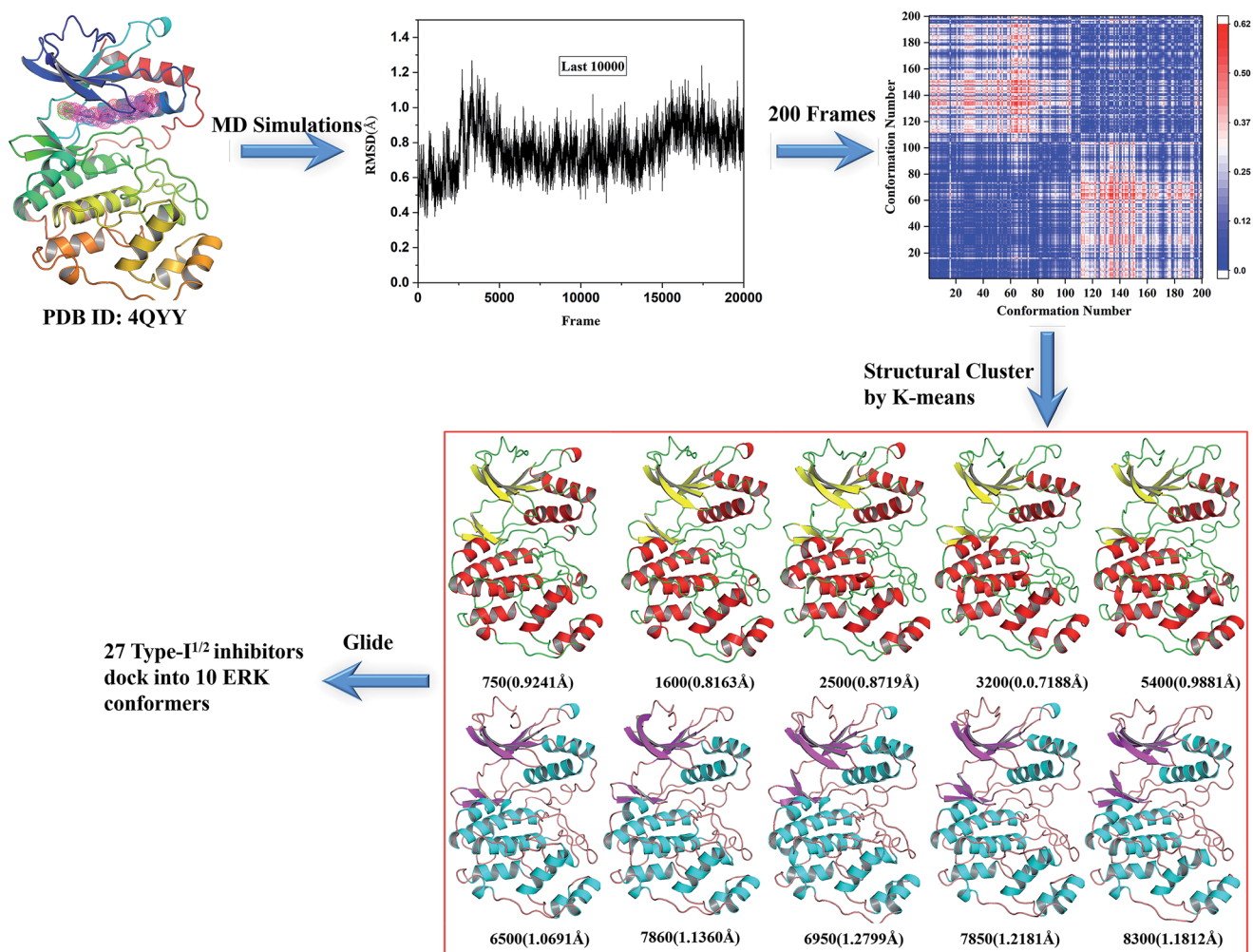


Fig. 3 Generation of the representative conformational ensembles base on 4QYY.

**2.3.2 Induced fit docking.** After obtained the best bound mode of ERK2 with every studies inhibitor, the induced fit docking (IFD) protocol was employed to investigate the importance of ERK2 flexibility to ligand binding. The best receptor–ligand complex was evaluated by the XP scoring and the side chains of the residues within 5 Å of each inhibitor is flexible.

**2.3.3 QM-polarized ligand docking.** The QM-Polarized Ligand Docking (QPLD) protocol in Schrodinger was employed to estimate the electrostatic interaction between receptor and ligand more accurately, which combines Glide and the QM/MM method implemented in Q-site. Based on the protein–ligand structures predicted by Glide, G-site computes the partial atomic charges with *ab initio* method and conducts a single-point energy calculation on each complex. Then, the binding poses are re-ranked based on the updated energies.

**2.3.4 Ensemble docking.** After 10 representative structures were generated from the MD simulations for each complex, the 27 inhibitors were successively docked into the 10 representative structures by using the RRD protocol with the XP scoring mode in Glide, and the pose with the best XP score was saved for each ligand.

## 2.4 Molecular dynamics (MD) simulations

The 27 ERK2-inhibitor complexes obtained by RRD based on the crystal structure of 4QYY were submitted to 5 ns NPT MD simulations ( $T = 300$  K and  $P = 1$  atm). For the details parameters setting of the MD simulations, please see the previous section “Generation of multiple representative ERK2 protein conformations”. The trajectory for each system was saved every 1 ps for the sampling process.

## 2.5 MM/PB(GB)SA binding free energy calculations and residue decomposition

The Molecular Mechanics/Poisson–Boltzmann Surface Area (MM/PBSA) and Molecular Mechanics/Generalized Born Surface Area (MM/GBSA) method,<sup>35,36</sup> widely used in elucidating receptor–ligand binding mechanisms,<sup>37–48</sup> were employed to estimate the ERK2-inhibitor binding free energies in AMBER14. In MM/PB(GB)SA, the binding free energy can be decomposed into several terms and 200 snapshots were extracted from the last 3 ns MD trajectory for the free energy

calculations. In MM/GBSA, the binding free energy can be calculated as follows:

$$\langle \Delta G_{\text{bind}} \rangle = \langle \Delta E_{\text{MM}} \rangle + \langle \Delta G_{\text{solvation}} \rangle - T \langle \Delta S_{\text{MM}} \rangle \quad (1)$$

where  $\langle \Delta G_{\text{bind}} \rangle$  is the calculated average free energy, and  $\langle \Delta E_{\text{MM}} \rangle$  is the average molecular mechanical energy.

$$\langle \Delta E_{\text{MM}} \rangle = \langle \Delta E_{\text{bond}} \rangle + \langle \Delta E_{\text{angle}} \rangle + \langle \Delta E_{\text{tors}} \rangle + \langle \Delta E_{\text{vdW}} \rangle + \langle \Delta E_{\text{elec}} \rangle \quad (2)$$

$$\langle \Delta G_{\text{solvation}} \rangle = \langle \Delta G_{\text{PB(GB)}} \rangle + \langle \Delta G_{\text{SA}} \rangle \quad (3)$$

$\langle \Delta G_{\text{solvation}} \rangle$  represents the desolvation free energy upon ligand binding, which is composed of the polar ( $\langle \Delta G_{\text{PB(GB)}} \rangle$ ) and nonpolar contributions ( $\langle \Delta G_{\text{SA}} \rangle$ ). The polar contribution of desolvation ( $\langle \Delta G_{\text{PB(GB)}} \rangle$ ) was calculated based on modified Generalized Born (GB) model ( $\text{igb} = 2$ ) developed by Onufriev and coworkers<sup>49</sup> or the PB model developed by Luo.<sup>50</sup> The solute dielectric constant was set to 1, and the solvent dielectric constant was set to 80. The LCPO method:  $\Delta G_{\text{SA}} = 0.0072 \times \Delta \text{SASA}$  was used to determine the nonpolar contribution ( $\langle \Delta G_{\text{SA}} \rangle$ ) of the desolvation by using solvent accessible surface area (SASA). The conformation entropy contribution can be calculated using normal-mode analysis, but considering high computational cost and low prediction accuracy, the calculated the conformational entropy contribution ( $-T \langle \Delta S \rangle$ ) upon ligand binding was neglected.<sup>51</sup>

Exploring the energy contribution of individual residue to the total binding free energy between the inhibitors and ERK2 is crucial, so the MM/GBSA binding free energy decomposition process<sup>52,53</sup> was used to decompose the interaction energy to each residue involved in the interaction by considering molecular mechanics and solvation energy without consideration of the contribution of entropy.

## 3. Results and discussion

### 3.1 Molecular docking based on the crystal structure

Redocking was used to verify the accuracy of our docking protocols for the two crystal structure 4QTA or 4QYY, which was implied by Glide with XP scoring mode in Schrodinger 2009. The RMSD between the binding pose and the corresponding

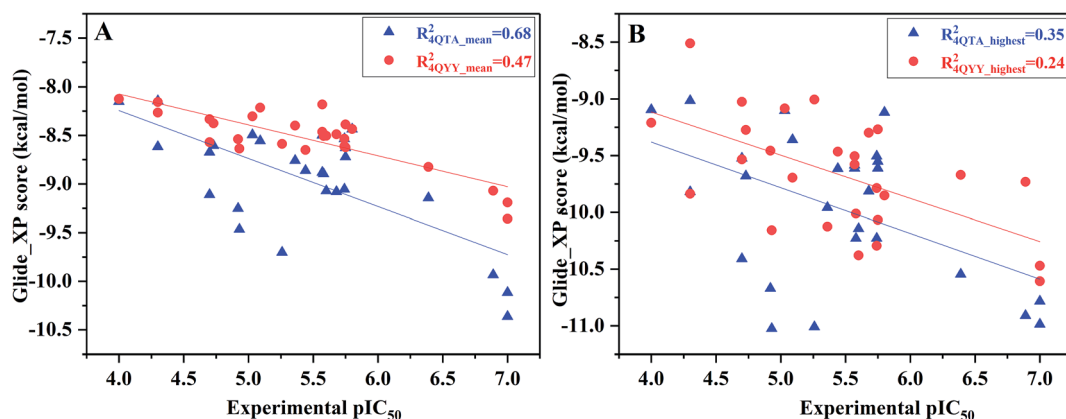


Fig. 4 Correlation between (A) the mean docking scores or (B) the highest docking scores predicted by ensemble docking and the experimental data.

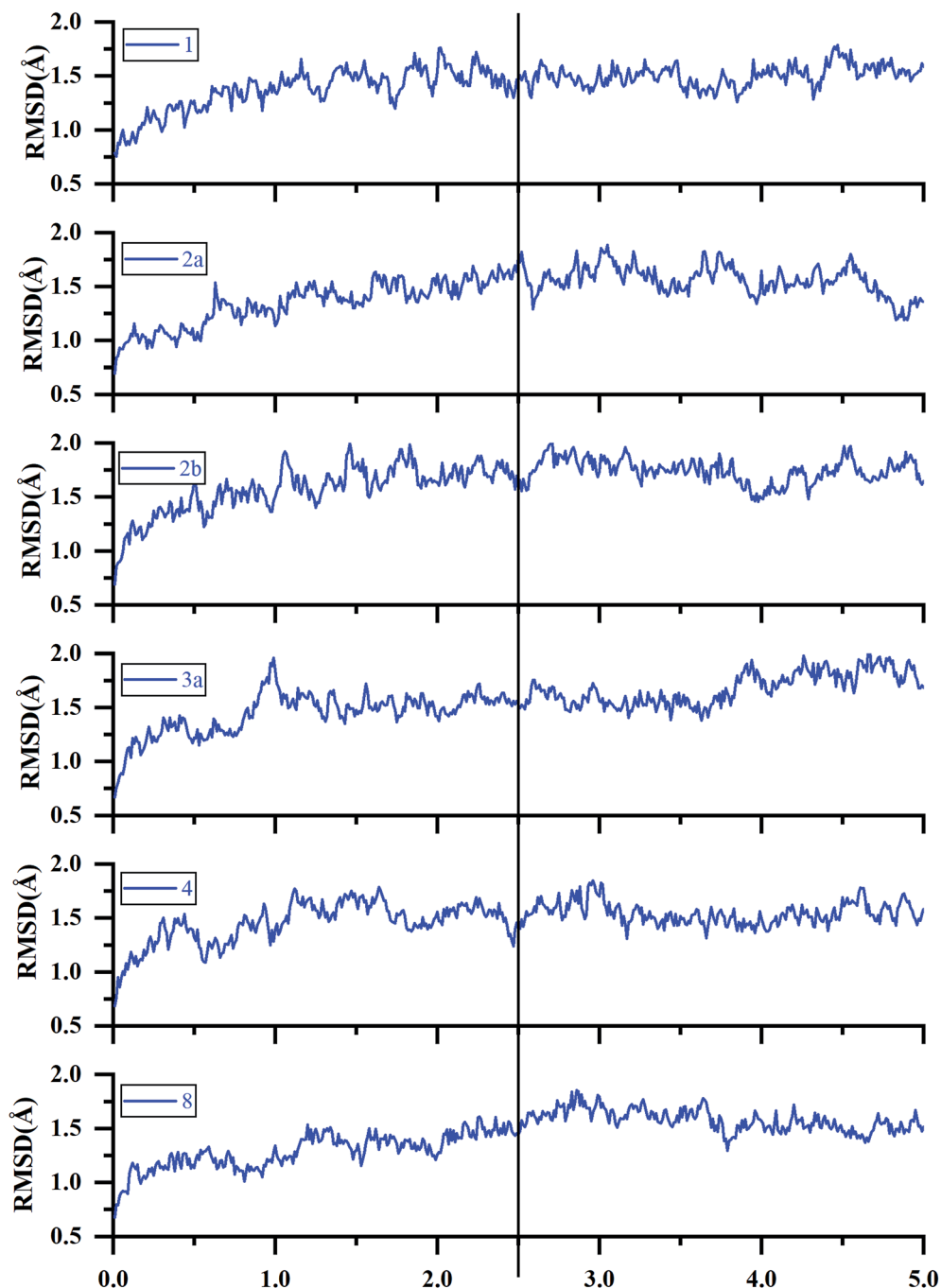


Fig. 5 RMSDs of the backbone C $\alpha$  atoms of the representative ERK2-inhibitors complexes (1, 2a, 2b, 3a, 4 and 8) as a function of simulation time.

experimental structure was 0.57 and 0.41 Å for 4QTA and 4QYY, respectively, indicating that the Glide RRD has high accuracy to reproduce the experimental binding poses.

Then, we docked all the 27 compounds into the active site of ERK2 (4QYY) in Schrodinger 2009, and three different docking protocols RRD, IFD and QPLD were implied. The corresponding docking scores are summarized in Table 1. The linear correlation between the experimental pIC<sub>50</sub> values and the docking scores was used to evaluate the performance of each docking protocol. As shown in Fig. 2, the correlation coefficient squares ( $R^2$ ) for RRD, IFD and QPLD are 0.08, 0.16 and 0.04, respectively.

The performance of IFD is better than those of RRD and QPLD, which mean that considering protein flexibility is a well method to enhance the docking accuracy. However, IFD can only considers the flexibility of residues around the active site, rather than the whole protein. Based on the above analysis, any of the traditional docking methods used above could not correctly rank the binding potencies with a high confidence.

### 3.2 Incorporating flexibility and dynamics into the receptor

**3.2.1 Docking into an ensemble of ERK2 conformations.** MD simulations have been proved to be a successful method to

obtain reasonable conformation of receptor–ligand interactions. Therefore, 20 ns MD simulations were employed for the two complexes, and the results show that after 10 ns, the RMSD of each system tends to converge, indicating that the systems are stable and equilibrated (Fig. S1†).

The *k*-means clustering algorithm were used to cluster 200 conformations extracted from the last stable 10 ns trajectory for each ERK2-inhibitors complex, at last 10 representative structures were eventually resolved for each complex (Fig. 3 and S2†). Then the 10 representatives as the receptor, 27 inhibitors were docked into the active site of ERK2 by using RRD. MD simulations generated most of conformations have better binding capability to rank the binding potency than the crystal structures (Fig. S3†), which indicates that the protein backbones of the conformations extracted from the MD simulations have obvious conformational rearrangement. Above analysis confirms the importance of protein flexibility on the prediction of protein–ligand interactions.

However, not all the binding capability of MD conformations is superior to the crystal structure ( $R_{4QTA_{4200}}^2 = 0.07$ ,  $R_{4QYY_{1600}}^2 = 0.00$ , and  $R_{4QYY_{5400}}^2 = 0.06$ ), which makes us wonder how to choose the reasonable conformation. In fact, it is difficult to determine the reasonable structures beforehand. Therefore, the highest and average docking scores of all the 10 representative conformations for each inhibitor were used to rank the binding affinities of the inhibitors (Fig. 4), which have better correlations ( $R_{4QTA_{mean}}^2 = 0.68$ ,  $R_{4QYY_{mean}}^2 = 0.47$ ,

$R_{4QTA_{highest}}^2 = 0.35$ , and  $R_{4QTA_{highest}}^2 = 0.24$ ) with the experimental data for the two crystal structures (4QTA and 4QYY). Obviously, the above results illustrate that the set of protein structures used in molecular docking can indeed improve the prediction accuracy.

**3.2.2 Binding free energy calculations based on the MD simulations of RRD docking results.** The binding complexes of the docked inhibitors based on the crystal structure 4QYY were used as the initial structures for 5 ns MD simulations due to the Glide docking shows better tolerance for the 27 inhibitors. The RMSDs and RMSF of the representative ERK2-inhibitor complexes (**1**, **2a**, **2b**, **3a**, **4**, and **8**) were analyzed to explore the overall stabilities during the MD simulations. As shown in Fig. 5 and 6, all the studied systems achieve equilibria after  $\sim 2.5$  ns. Most of the residues with greater flexibility are located in the loop regions, such as P-loop. The residues located in the ATP binding pocket and allosteric pocket bear relatively higher rigidity because they form strong interactions with inhibitors.

The binding free energies and the energy components for each inhibitor-ERK2 system were predicted based on the 200 snapshots using the MM/PBSA and MM/GBSA approaches. Fig. 7 the shows that MM/PBSA ( $R^2 = 0.43$ ) is superior than that of MM/GBSA ( $R^2 = 0.33$ ) in predicting receptor and ligand binding affinity, but both methods perform better than RRD, IFD, QPLD and even ensemble docking. In addition, the correlations between the individual energy terms and the experimental activities were compared (Fig. S4†). The results show

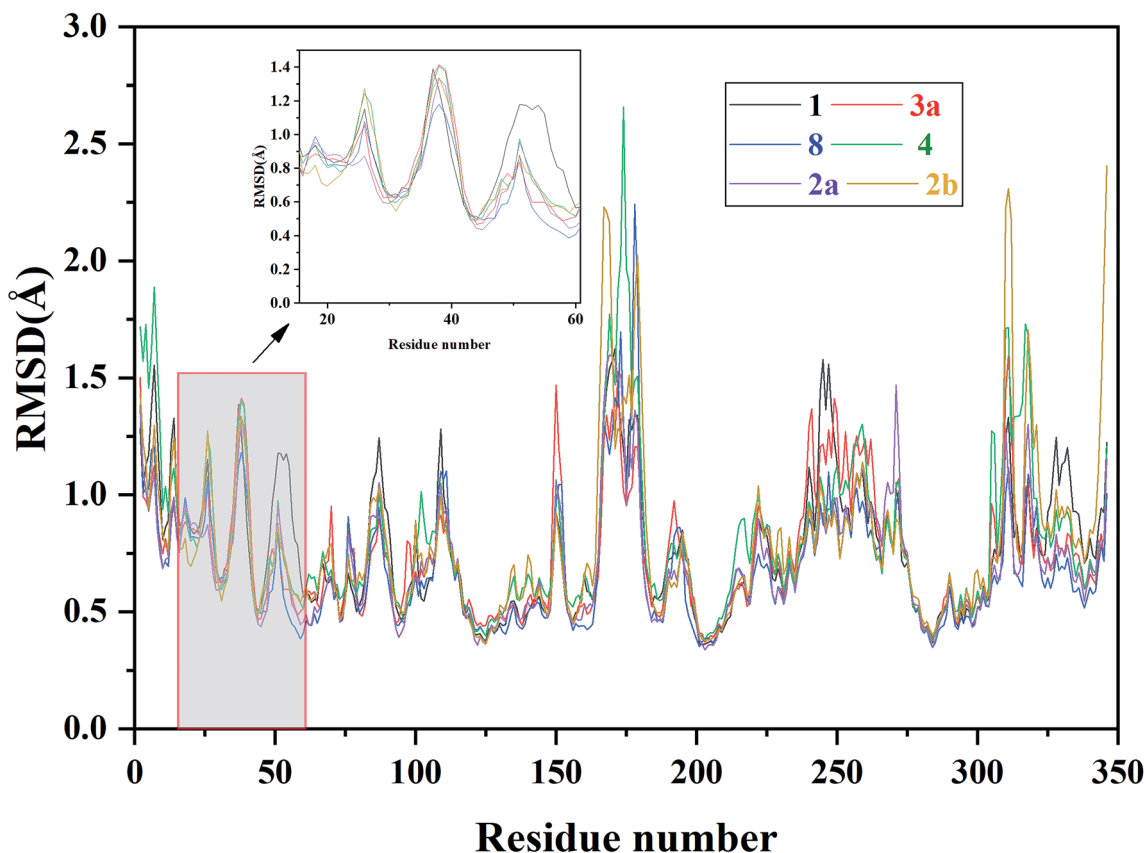


Fig. 6 RMSF of each residue of the selected ERK2-inhibitors complexes (**1**, **2a**, **2b**, **3a**, **4** and **8**) obtained from the MD simulations.



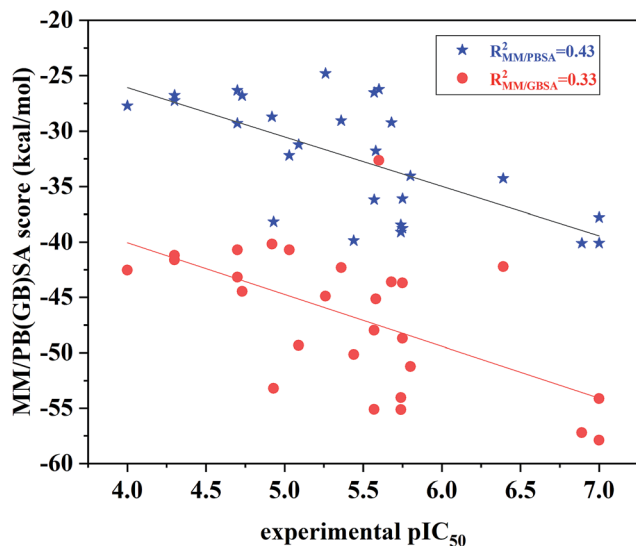


Fig. 7 Correlation between the binding free energies calculated by MM/PBSA or MM/GBSA and the experimental data.

that the linear correlations between the non-polar ( $\Delta E_{\text{vdw}} + \Delta G_{\text{SA}}$ ; MM/PBSA:  $R^2 = 0.33$ ) contributions and the experimental data is significantly higher than that of the polar contributions ( $\Delta E_{\text{ele}} + \Delta G_{\text{PB}}$ ; MM/GBSA:  $R^2 = 0.06$ ) and the experimental data. As a conclusion, the non-polar contributions are possibly more important than the polar contributions to determine the discrepancy of the binding affinities of the 27 inhibitors.

Furthermore, as shown in Table 2, the predicted binding affinity of compound **1** ( $-32.78 \text{ kcal mol}^{-1}$ ) is stronger than those of the derivatives bound with the allosteric pocket (**2-3d**) or ATP binding pocket (**1a, 9-9d**) and modifications, which is consistent with the experimental results. In addition, the compounds with different terminal substitutions located in the allosteric pocket (**2-2b, 3, 4** and **5**) display different binding affinities compared with compound **1**. The above results predicted by MM/PBSA are basically accordant to the experimental data.

### 3.3 Identification of key residues responsible for inhibitor binding

In order to further identify the key residues for ERK2 binding to inhibitors, as well as understand the possible molecular mechanism of the important substituents that can improve the binding affinity with ERK2, the enthalpy ( $\Delta G_{\text{bind,PB}}$ ) of representative inhibitors (**1, 2a, 2b, 4** and **8**) was decomposed into a per-residue depicted in Fig. 8. According to Fig. 8, the key residues contributing to the binding progress is: Val37, Lys52, Ile82, Gln103, Leu105, Met106 and Leu154 (the ATP binding pocket) and Tyr34, Pro56, Tyr62, Asp165, Phe166 and Val186 (the allosteric pocket), and the main role of these residues for ERK2 binding inhibitors are hydrogen bonding and hydrophobic interaction. The contributions of the non-polar residues are a very important part of the binding free energies, especially the residues Val37, Lys52, Tyr62, Arg65, Glu69, Met106 and

Table 2 Binding free energies and individual energy components predicted by MM/PBSA ( $\text{kcal mol}^{-1}$ )

System	$\Delta E_{\text{ele}}$	$\Delta E_{\text{vdw}}$	$\Delta G_{\text{PB}}$	$\Delta G_{\text{SA}}$	$\Delta G_{\text{nonpolar}}^a$	$\Delta G_{\text{polar}}^b$	$\Delta G_{\text{bind,PB}}$	pIC <sub>50</sub>
ERK2/1	-74.22	-54.34	104.88	-9.10	-63.44	30.66	-32.78	5.58
ERK2/1a	-73.13	-52.84	104.97	-7.64	-60.48	31.84	-28.64	5.68
ERK2/1b	47.81	-53.31	98.02	-8.11	-61.42	30.21	-31.21	5.09
ERK2/2	-52.89	-61.56	94.26	-8.86	-70.42	41.37	-29.05	5.36
ERK2/2a	-59.32	-51.26	91.88	-9.00	-60.26	32.56	-27.70	4.00
ERK2/2b	-66.49	-54.66	103.00	-8.61	-63.27	36.51	-26.76	4.30
ERK2/3	-66.77	-50.93	98.08	-8.74	-59.67	33.36	-26.31	4.70
ERK2/3a	-64.72	-57.09	105.51	-8.52	-65.61	40.79	-24.82	5.26
ERK2/3b	-51.96	-69.80	92.47	-8.68	-78.48	40.51	-29.28	4.70
ERK2/3c	-63.20	-67.42	114.09	-8.53	-75.95	46.67	-28.69	4.92
ERK2/3d	-58.44	-61.09	95.26	-7.92	-69.01	36.82	-32.19	5.03
ERK2/4	-78.24	-65.10	117.55	-8.46	-73.56	39.31	-34.26	6.39
ERK2/4a	-68.93	-64.12	103.23	-7.97	-72.09	34.30	-37.79	7.00
ERK2/4b	-67.89	-73.49	104.63	-8.63	-82.12	43.37	-38.75	5.75
ERK2/5	-57.65	-65.72	93.18	-8.92	-74.64	35.54	-39.10	5.74
ERK2/5a	-58.80	-64.89	96.57	-9.07	-73.96	37.77	-36.19	5.57
ERK2/6	-64.70	-71.80	104.94	-8.55	-80.35	40.24	-40.11	6.89
ERK2/7	-67.42	-73.76	107.69	-8.41	-82.17	40.27	-40.10	7.00
ERK2/7a	-58.99	-64.88	96.46	-9.21	-74.09	37.47	-36.62	5.75
ERK2/7b	-73.65	-68.07	112.38	-9.10	-77.17	38.73	-38.44	5.74
ERK2/7c	-58.29	-58.20	97.91	-7.62	-65.82	39.32	-26.50	5.57
ERK2/8	-56.50	-63.96	94.39	-7.97	-71.93	37.89	-34.04	5.80
ERK2/9	-68.36	-58.89	108.38	-7.91	-66.80	35.02	-31.78	4.73
ERK2/9a	-67.01	-51.33	99.44	-8.33	-59.66	32.43	-27.23	4.30
ERK2/9b	-70.46	-71.94	111.46	-8.93	-80.87	41.00	-39.87	5.44
ERK2/9c	-55.37	-63.32	88.74	-8.22	-71.54	33.37	-38.17	4.93
ERK2/9d	-71.09	-60.30	103.28	-8.10	-68.40	32.19	-26.21	5.60

$$^a \Delta G_{\text{polar}} = \Delta E_{\text{ele}} + \Delta G_{\text{PB}}, \quad ^b \Delta G_{\text{nonpolar}} = \Delta E_{\text{vdw}} + \Delta G_{\text{SA}}$$

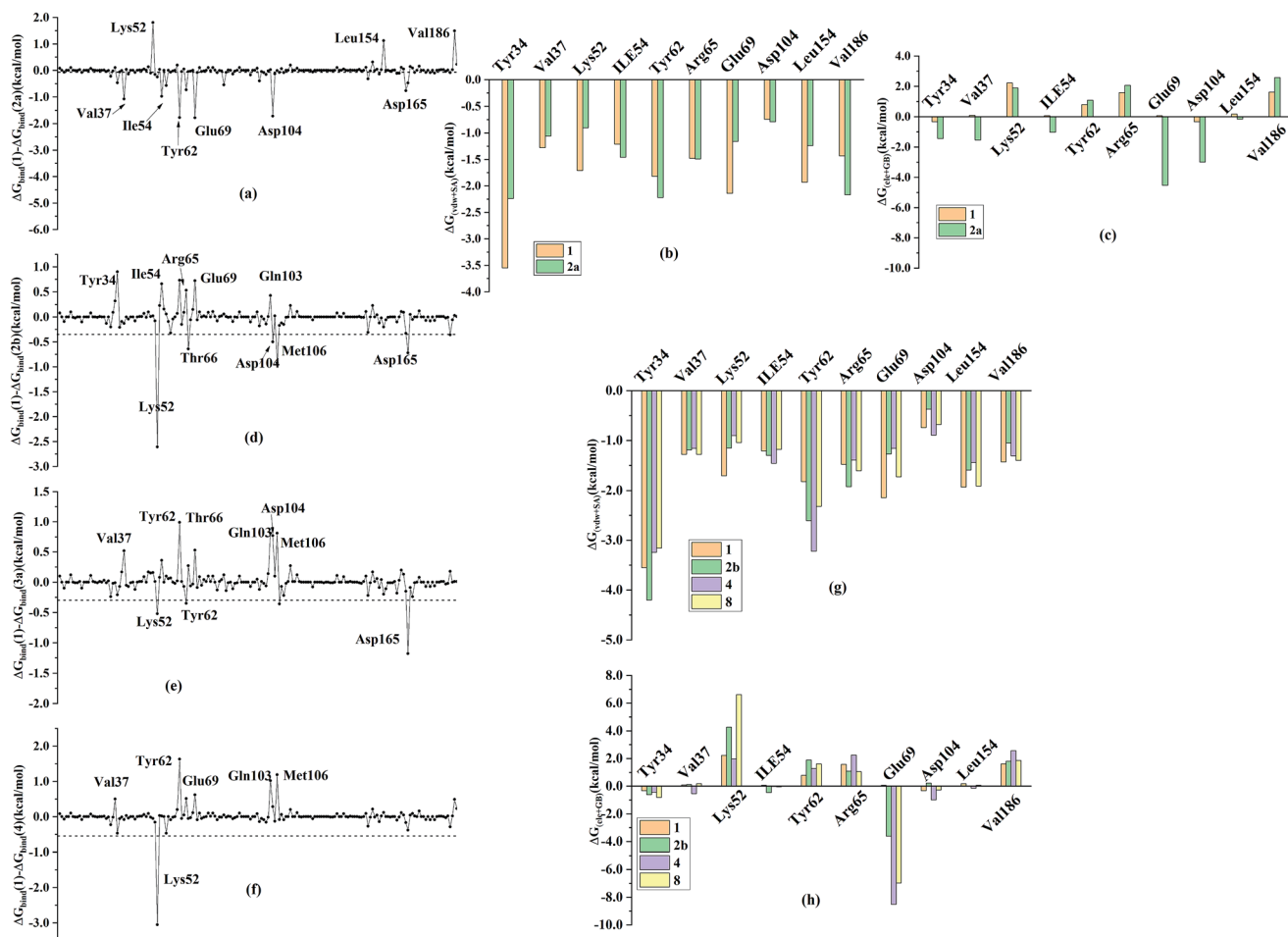


Fig. 8 Comparison of the inhibitor–residue interaction energies of compounds 1 and (a) 2a, (d) 2b, (e) 4 and (f) 8; comparison of the (b) non-polar and (c) polar interactions of compounds 1 and 2a, comparison of the (g) non-polar and (h) polar interactions of compounds 1 and 2b, 4 and 8.

Leu154. The contributions of the polar residues (e.g. Tyr34, Ile54, Met106 and Asp165) are relatively insignificant except for the residues Lys52 and Tyr62, and there is a slight energetic difference between different inhibitors. The  $\text{pIC}_{50}$  values of the compounds 2b, 4 and 8 are about 20 times higher than that of compound 1, while compound 2a shows the lowest activity. Structural analysis shows that these compounds have different substituents interacting with the allosteric pocket region. By further comparing the binding characteristics of the selected inhibitors, we can understand the structural requirements of inhibitors for enhancing binding affinity, which will guide the rational design of more effective and selective ERK2 Type I<sup>1/2</sup> inhibitors.

**3.3.1 Comparison of bound modes of 1 and 2a.** The replacement of the acetyl group in compound 1 by fluorophenyl (compound 2a) at the allosteric pocket significantly decreases the binding affinity. According to the Table 2, the predicted binding free energy of 1 ( $-32.78 \text{ kcal mol}^{-1}$ ) is much stronger than that of 2a ( $-27.70 \text{ kcal mol}^{-1}$ ), which is consistent with the experimental data. The difference of the unfavorable polar contributions between 2a ( $32.56 \text{ kcal mol}^{-1}$ ) and 1 ( $30.66 \text{ kcal mol}^{-1}$ ) is  $1.9 \text{ kcal mol}^{-1}$ , while the difference of the

non-polar contributions between compounds 1 ( $-63.44 \text{ kcal mol}^{-1}$ ) and 2a ( $-60.26 \text{ kcal mol}^{-1}$ ) is  $3.18 \text{ kcal mol}^{-1}$  (Table 2). The difference of the energy contributions of Tyr62 between 1 and 2a is the largest ( $-1.77 \text{ kcal mol}^{-1}$ ). This is because the acetyl group in compound 1 can form stronger non-polar interactions with Tyr62 than the fluorophenyl substituent in 2a (Fig. 9). Besides, the contributions of the residues located in the ATP binding pocket (Tyr34, Val37, Lys52 and Ile54) and Asp165 to the binding of compound 1 are higher than those to the binding of compound 2a, but the difference is not obvious. As shown in Fig. 8, the two compounds form effective interactions with the residues Tyr34, Lys52, Tyr62, Gln103 and Met106, and these residues mainly locate in the ATP binding pocket and the allosteric pocket. The replacement of the acetyl group in compound 1 by fluorophenyl substituent may result in the conformational change of the inhibitors, which lead to the formation of more effective interactions with several residues far away from the allosteric pocket, such as residue Val186. In addition, the residues Glu69 and Asp104 have difference in non-polar interactions (Fig. 8(b) and (c)), which also may play a critical role in rendering the difference of the binding free energies.

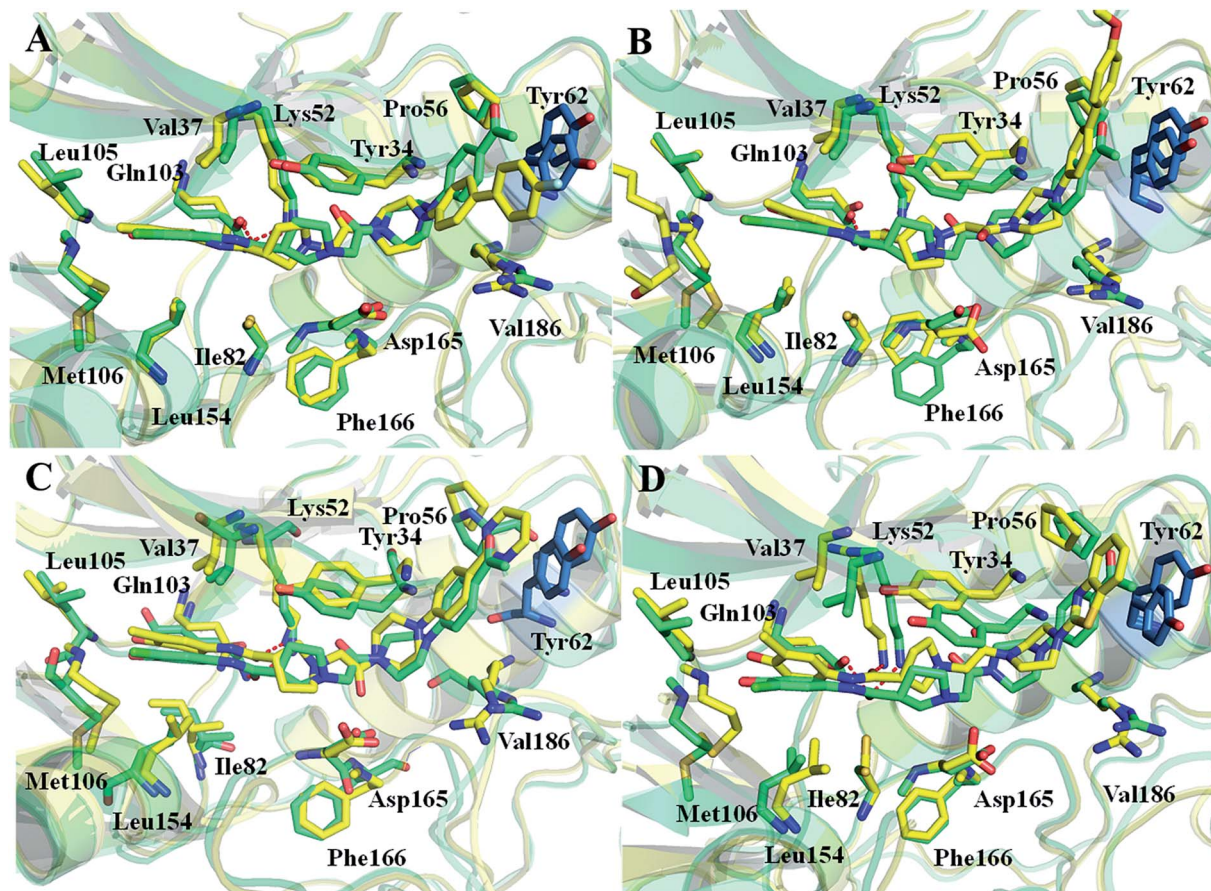


Fig. 9 Comparison of the averaged structures of (A) compounds 1 and 2a, (B) compounds 1 and 2b, (C) compounds 1 and 4, and (D) compounds 1 and 8.

**3.3.2 Comparison of binding modes of 1, 2b, 4 and 8.** Different terminal substitutions of compounds 1, 2b, 4 and 8 mainly occupy the allosteric pocket of ERK2. The binding free energies of 4 and 8 predicted by MM/PBSA are relatively stronger than that of compound 1 while that of 2b is weaker than that of compound 1, which is closely consistent with the experimental data. The Fig. 8(e) and (f) show that almost all the residues Val37, Lys52, Ile82, Leu105, Met106 and Leu154 have stronger interactions with compounds 4 and 8 than with compound 1, are these residues are hydrophobic and they are located in ATP binding pocket. Detailed analysis indicates that the contributions of Val37, Gln103 and Met106 located in the ATP binding pocket to the binding of compound 1 are obviously weaker than those to the binding of the compounds 4 and 8 (the differences between compound 1 and 4 for Val37, Gln103 and Met106 are 0.49, 0.77 and 0.81 kcal mol<sup>-1</sup>, respectively; the differences between compound 1 and 8 for Val37, Gln103 and Met106 are 0.5, 0.43 and 1.02 kcal mol<sup>-1</sup>, respectively) (Fig. 9(g) and (h)). In addition, the contributions of the residues Tyr62 and Gln69 to the compounds 4 and 8 binding are more favorable than those to the compound 1 binding, which can be explained by the fact that the residues Tyr62 and Gln69 tend to form stronger interactions with the terminal substitutions of 4 and 8 (Fig. 9(C) and (D)). Detailed structure analysis indicates that the  $\pi$ - $\pi$  interaction between the Tyr62 side chain and the terminal substitutions of compounds 4

and 8 is stronger than that of compound 1. However, the predicted binding free energy of compound 2b is weaker than that of compound 1, which is supported by the per-residue energy decomposition analysis that Lys52, Thr66, Met106 and Asp165 show more favorable contribution to compound 1 binding than to compound 2b binding (the differences for Lys52, Thr66, Met106 and Asp165 are 2.61, 0.64, 0.92 and 0.72, respectively) (Fig. 8(d)), and also is supported by the detailed structure analysis that the instability of the large terminal substitution of compound 2b with the allosteric pocket (Fig. 9(B)).

### 3.4 Suggestions for designing of improved Type I<sup>1/2</sup> ERK2 inhibitors

Based on the binding free energy calculations and structural analysis, we could propose several improved design criterions for Type I<sup>1/2</sup> ERK2 inhibitors.

(1) Considering the flexibility and dynamics behavior of ERK2 is quite important to correctly predict the binding potencies of Type I<sup>1/2</sup> inhibitors. MD simulations is an important way to improve protein flexibility, and the results indicate that the protein structures obtained from the MD simulations show better tolerance to the ligands. Meanwhile, MD simulations can obviously improve the ranking ability of the binding potencies of the studied ERK2 inhibitors. The binding affinities give the best correlation with the

experimental data, which highlighting the importance of incorporating protein flexibility in predicting ERK2-inhibitors interactions.

(2) The hydrogen bonds between the side chain of residues Lys52 and Gln103 with inhibitors play a key role in stabilizing the interaction between inhibitors and ERK2. The favorable van der Waals contribution ( $\Delta E_{vdw}$ ) is important for improving the interaction between ERK2 and inhibitors, which mainly contributes the non-polar interaction. The hydrophobic contributions may be highly helpful to improve the binding ability of ERK2 inhibitors, and the hydrophobic contributions are mainly from some surrounding key residues, such as Val37, Gln103, Asp104 and Met106. Therefore, potential improved ERK2 inhibitors can be designed by increasing hydrophobic interactions, as well as keeping the hydrogen bounds between ERK2 and ERK2 inhibitors.

(3) The terminal substitute interacts “face to face” with the residue Tyr62 side chain through an aromatic  $\pi$ - $\pi$  interaction is of significant importance for improving activities of ERK2 inhibitors. The results given by our calculations and the experimental data show that large terminal substitute is unfavorable for inhibitors, for example compound **2a**.

## 4. Conclusions

In this work, the binding mechanisms of ERK2 with the Type I<sup>1/2</sup> inhibitors were investigate by molecular docking, ensemble docking, MD simulations and binding free energy calculations. Our prediction results show that it is necessary to consider the flexibility of receptor before performing molecular docking to improve the prediction accuracy of traditional docking methods, such as Glide docking, IFD and QPLD. In particular, MD simulations is a well way to improve the flexibility and the binding free energies predicted by MM/PBSA protocols show the highest correlation with the experimental data, which investigates the importance of protein flexibility to predict ERK2 with the Type I<sup>1/2</sup> inhibitors interactions. The results of binding free energy calculations predicted by MM/PBSA show that the non-polar interactions play determinative roles in the binding of ERK2 inhibitors, which leads to the difference of the binding affinities of the inhibitors. Several possible key residues for inhibitors binding are identified by the binding free energy decomposition analysis. In addition, the comprehensive analysis of several representative inhibitors also demonstrates the importance of hydrophobic and hydrogen bonds interactions between the residues located in the ATP binding pocket and the allosteric pocket and the inhibitors in improving the binding affinities of the inhibitors. We hope our results will provide a deeper understanding of the interaction between the Type I<sup>1/2</sup> inhibitors and ERK2 more valuable information for the further design of new potent ERK2 inhibitors.

## Conflicts of interest

The authors declare that there is no conflict of interest in this work.

## Acknowledgements

This work was supported by the Natural Foundation of Shandong Province (Grant No. ZR2018BB055).

## References

- 1 O. K. Mirzoeva, D. Das, L. M. Heiser, *et al.*, Basal Subtype and MAPK/ERK Kinase (MEK)-Phosphoinositide 3-Kinase Feedback Signaling Determine Susceptibility of Breast Cancer Cells to MEK Inhibition, *Cancer Res.*, 2009, **69**, 565–572.
- 2 N. Sawe, G. Steinberg and H. Zhao, Dual roles of the MAPK/ERK1/2 cell signaling pathway after stroke, *J. Neurosci. Res.*, 2008, **86**, 1659.
- 3 P. Y. Yeh, S. E. Chuang, K. H. Yeh, *et al.*, Increase of the resistance of human cervical carcinoma cells to cisplatin by inhibition of the MEK to ERK signaling pathway partly via enhancement of anticancer drug-induced NF kappa B activation, *Biochem. Pharmacol.*, 2002, **63**, 1423–1430.
- 4 P. J. Roberts and C. J. Der, Targeting the Raf-MEK-ERK mitogen-activated protein kinase cascade for the treatment of cancer, *Oncogene*, 2007, **26**, 3291–3310.
- 5 S. Schubert, K. Shannon and G. Bollag, Hyperactive Ras in developmental disorders and cancer, *Nat. Rev. Cancer*, 2007, **7**, 295–308.
- 6 S. Wilhelm, C. Carter, M. Lynch, *et al.*, Discovery and development of sorafenib: a multikinase inhibitor for treating cancer, *Nat. Rev. Drug Discovery*, 2006, **5**, 835.
- 7 F. Romerio and D. Zella, MEK and ERK inhibitors enhance the antiproliferative effect of interferon- $\alpha$ 2b, *FASEB J.*, 2002, **16**, 1680.
- 8 M. S. Carlino, J. R. Todd, K. Gowrishankar, *et al.*, Differential activity of MEK and ERK inhibitors in BRAF inhibitor resistant melanoma, *Mol. Oncol.*, 2014, **8**, 544–554.
- 9 A. M. Aronov, C. Baker, G. W. Bemis, *et al.*, Flipped out: structure-guided design of selective pyrazolopyrrole ERK inhibitors, *J. Med. Chem.*, 2007, **50**, 1280–1287.
- 10 M. Otori, T. Kinoshita, M. Okubo, *et al.*, Identification of a selective ERK inhibitor and structural determination of the inhibitor-ERK2 complex, *Biochem. Biophys. Res. Commun.*, 2005, **336**, 357–363.
- 11 E. J. Morris, S. Jha, C. R. Restaino, *et al.*, Discovery of a novel ERK inhibitor with activity in models of acquired resistance to BRAF and MEK inhibitors, *Cancer Discovery*, 2013, **3**, 742–750.
- 12 A. M. Aronov, Q. Tang, G. Martinez-Botella, *et al.*, Structure-guided design of potent and selective pyrimidylpyrrole inhibitors of extracellular signal-regulated kinase (ERK) using conformational control, *J. Med. Chem.*, 2009, **52**, 6362–6368.
- 13 J. F. Blake, M. Burkard, J. Chan, *et al.*, Discovery of (S)-1-(1-(4-chloro-3-fluorophenyl)-2-hydroxyethyl)-4-(2-((1-methyl-1H-pyrazol-5-yl)amino)pyrimidin-4-yl)pyridin-2(1H)-one (GDC-0994), an extracellular signal-regulated kinase 1/2 (ERK1/2) inhibitor in early clinical development, *J. Med. Chem.*, 2016, **59**, 5650–5660.
- 14 Y. Niu, D. Pan, Y. Yang, *et al.*, Revealing the molecular mechanism of different residence times of ERK2 inhibitors via binding free energy calculation and unbinding pathway analysis, *Chemom. Intell. Lab. Syst.*, 2016, **158**, 91–101.

- 15 T. Zhang, Y. Liu, X. Yang, *et al.*, Definitive Metabolite Identification Coupled with Automated Ligand Identification System (ALIS) Technology: A Novel Approach to Uncover Structure-Activity Relationships and Guide Drug Design in a Factor IXa Inhibitor Program, *J. Med. Chem.*, 2016, **59**, 1818.
- 16 Y. Deng, G. W. Shippy, A. Cooper, *et al.*, Discovery of Novel, Dual Mechanism ERK Inhibitors by Affinity Selection Screening of an Inactive Kinase, *J. Med. Chem.*, 2014, **57**, 8817–8826.
- 17 X. Kong, P. Pan, D. Li, *et al.*, Importance of protein flexibility in ranking inhibitor affinities: modeling the binding mechanisms of piperidine carboxamides as Type I1/2 ALK inhibitors, *Phys. Chem. Chem. Phys.*, 2015, **17**, 6098–6113.
- 18 X. Kong, H. Sun, P. Pan, *et al.*, Importance of protein flexibility in molecular recognition: a case study on Type-I<sup>1/2</sup> inhibitors of ALK, *Phys. Chem. Chem. Phys.*, 2018, **20**, 4851–4863.
- 19 P. Pan, H. Yu, Q. Liu, *et al.*, Combating Drug-Resistant Mutants of Anaplastic Lymphoma Kinase with Potent and Selective Type-I<sup>1/2</sup> Inhibitors by Stabilizing Unique DFG-Shifted Loop Conformation, *ACS Cent. Sci.*, 2017, **3**, 1208–1220.
- 20 S. Tian, H. Sun, Y. Li, *et al.*, Development and evaluation of an integrated virtual screening strategy by combining molecular docking and pharmacophore searching based on multiple protein structures, *J. Chem. Inf. Model.*, 2013, **53**, 2743–2756.
- 21 S. Tian, H. Sun, P. Pan, *et al.*, Assessing an ensemble docking-based virtual screening strategy for kinase targets by considering protein flexibility, *J. Chem. Inf. Model.*, 2014, **54**, 2664–2679.
- 22 A. Chaikuad, E. M. C. Tacconi, J. Zimmer, *et al.*, A unique inhibitor binding site in ERK1/2 is associated with slow binding kinetics, *Nat. Chem. Biol.*, 2014, **10**, 853.
- 23 *Prime, version 2.0*, Schrödinger, LLC, New York, 2008.
- 24 Y. Zhu, J. Desai, Y. Deng, *et al.*, Discovery of hydroxyaniline amides as selective extracellular regulated kinase (Erk) inhibitors, *Bioorg. Med. Chem. Lett.*, 2015, **25**, 1627–1629.
- 25 G. A. K. And, R. A. Friesner, T. R. And, *et al.*, Evaluation and reparametrization of the OPLS-AA force field for proteins via comparison with accurate quantum chemical calculations on peptides, *J. Phys. Chem. B*, 2001, **105**, 6474–6487.
- 26 P. Cieplak, W. D. Cornell, C. Bayly, *et al.*, Application of the multimolecule and multiconformational RESP methodology to biopolymers: charge derivation for DNA, RNA, and proteins, *J. Comput. Chem.*, 1995, **16**, 1357–1377.
- 27 C. I. Bayly, P. Cieplak, W. Cornell, *et al.*, A well-behaved electrostatic potential based method using charge restraints for deriving atomic charges: the RESP model, *J. Phys. Chem.*, 1993, **97**, 10269–10280.
- 28 T. Fox and P. A. Kollman, Application of the RESP Methodology in the Parametrization of Organic Solvents, *J. Phys. Chem.*, 1998, **102**, 8070–8079.
- 29 K. Lindorff-Larsen, S. Piana, K. Palmo, *et al.*, Improved side-chain torsion potentials for the Amber ff99SB protein force field, *Proteins: Struct., Funct., Bioinf.*, 2010, **78**, 1950–1958.
- 30 J. Wang, R. M. Wolf, J. W. Caldwell, *et al.*, Development and testing of a general amber force field, *J. Comput. Chem.*, 2004, **25**, 1157–1174.
- 31 W. L. Jorgensen, J. Chandrasekhar, J. D. Madura, *et al.*, Comparison of simple potential functions for simulating liquid water, *J. Chem. Phys.*, 1983, **79**, 926–935.
- 32 Y. Niu, D. Shi, L. Li, *et al.*, Revealing inhibition difference between PFI-2 enantiomers against SETD7 by molecular dynamics simulations, binding free energy calculations and unbinding pathway analysis, *Sci. Rep.*, 2017, **7**, 46547.
- 33 J. C. Phillips, R. Braun, W. Wang, *et al.*, Scalable molecular dynamics with NAMD, *J. Comput. Chem.*, 2005, **26**, 1781–1802.
- 34 T. Darden, D. York and L. Pedersen, Particle mesh Ewald: an N·log(N) method for Ewald sums in large systems, *J. Chem. Phys.*, 1993, **98**, 10089–10092.
- 35 P. A. Kollman, I. Massova, C. Reyes, *et al.*, Calculating structures and free energies of complex molecules: combining molecular mechanics and continuum models, *Acc. Chem. Res.*, 2000, **33**, 889–897.
- 36 P. D. Lyne, M. L. Lamb and J. C. Saeh, Accurate prediction of the relative potencies of members of a series of kinase inhibitors using molecular docking and MM-GBSA scoring, *J. Med. Chem.*, 2006, **49**, 4805–4808.
- 37 J.-P. Ryckaert, G. Ciccotti and H. J. C. Berendsen, Numerical integration of the cartesian equations of motion of a system with constraints: molecular dynamics of n-alkanes, *J. Comput. Phys.*, 1977, **23**, 327–341.
- 38 A. Weis, K. Katebzadeh, P. Söderhjelm, *et al.*, Ligand affinities predicted with the MM/PBSA method: dependence on the simulation method and the force field, *J. Med. Chem.*, 2006, **49**, 6596.
- 39 P. A. Kollman, I. Massova, C. Reyes, *et al.*, Calculating structures and free energies of complex molecules: Combining molecular mechanics and continuum models, *Acc. Chem. Res.*, 2000, **33**, 889–897.
- 40 J. Galvez, S. Polo, B. Insuasty, *et al.*, Design, facile synthesis, and evaluation of novel spiro- and pyrazolo1,5-c quinazolines as cholinesterase inhibitors: molecular docking and MM/GBSA studies, *Comput. Biol. Chem.*, 2018, **74**, 218–229.
- 41 H. Sun, L. Duan, F. Chen, *et al.*, Assessing the performance of MM/PBSA and MM/GBSA methods. 7. entropy effects on the performance of end-point binding free energy calculation approaches, *Phys. Chem. Chem. Phys.*, 2018, **20**, 14450–14460.
- 42 T. Hou, J. Wang, Y. Li, *et al.*, Assessing the performance of the molecular mechanics/Poisson Boltzmann surface area and molecular mechanics/generalized Born surface area methods. II. The accuracy of ranking poses generated from docking, *J. Comput. Chem.*, 2011, **32**, 866–877.
- 43 H. Sun, Y. Li, S. Tian, *et al.*, Assessing the performance of MM/PBSA and MM/GBSA methods. 4. Accuracies of MM/PBSA and MM/GBSA methodologies evaluated by various simulation protocols using PDBbind data set, *Phys. Chem. Chem. Phys.*, 2014, **16**, 16719–16729.

- 44 J. Wang, T. Hou and X. Xu, Recent Advances in Free Energy Calculations with a Combination of Molecular Mechanics and Continuum Models, *Curr. Comput.-Aided Drug Des.*, 2006, **2**, 95–103.
- 45 L. Xu, H. Sun, Y. Li, *et al.*, Assessing the performance of MM/PBSA and MM/GBSA methods. 3. The impact of force fields and ligand charge models, *J. Phys. Chem. B*, 2013, **117**, 8408–8421.
- 46 H. Sun, Y. Li, S. Tian, *et al.*, P-loop conformation governed crizotinib resistance in G2032R-mutated ROS1 tyrosine kinase: clues from free energy landscape, *PLoS Comput. Biol.*, 2014, **10**, e1003729.
- 47 H. Sun, Y. Li, M. Shen, *et al.*, Assessing the performance of MM/PBSA and MM/GBSA methods. 5. Improved docking performance using high solute dielectric constant MM/GBSA and MM/PBSA rescoring, *Phys. Chem. Chem. Phys.*, 2014, **16**, 22035–22045.
- 48 N. Homeyer and H. Gohlke, Free Energy Calculations by the Molecular Mechanics Poisson-Boltzmann Surface Area Method, *Mol. Inf.*, 2012, **31**, 114–122.
- 49 A. Onufriev, D. Bashford and D. A. Case, Exploring protein native states and large-scale conformational changes with a modified generalized born model, *Proteins: Struct., Funct., Bioinf.*, 2004, **55**, 383–394.
- 50 Q. Lu and R. Luo, Analyzing the biopolymer folding rates and pathways using kinetic cluster method, *J. Chem. Phys.*, 2003, **119**, 11035–11048.
- 51 T. Hou, J. Wang, Y. Li, *et al.*, Assessing the performance of the MM/PBSA and MM/GBSA methods. 1. The accuracy of binding free energy calculations based on molecular dynamics simulations, *J. Chem. Inf. Model.*, 2011, **51**, 69–82.
- 52 T. Hou, N. Li, Y. Li, *et al.*, Characterization of domain-peptide interaction interface: prediction of SH3 domain-mediated protein-protein interaction network in yeast by generic structure-based models, *J. Proteome Res.*, 2012, **11**, 2982–2995.
- 53 G. Holger, K. Christina and A. C. David, Insights into protein-protein binding by binding free energy calculation and free energy decomposition for the Ras-Raf and Ras-RalGDS complexes, *J. Mol. Biol.*, 2003, **330**, 891–913.